Effect of Grain Shape and Relative Humidity on the Nonlinear Elastic Properties of Granular Media

L. Gao[1], P. Shokouhi[1], and J. Rivière[1]

[1] Department of Engineering Science and Mechanics, Pennsylvania State University, University Park, Pennsylvania 16802, USA.

Corresponding author: Linying Gao(lzg245@psu.edu)

Key Points:

- The elastic nonlinearity of angular, fine sand particles is rather independent of relativity humidity (RH) level.
- This is in contrast with observations made in spherical glass beads, which show an increase in elastic nonlinearity with RH.
- We attribute this RH independence in sand to grain interlocking that prevents adsorbed water from weakening the grain junctions.

Abstract

This study focuses on unraveling the microphysical origins of the nonlinear elastic effects, which are pervasive in the Earth's crust. Here, we examine the influence of grain shape on the elastic nonlinearity of granular assemblies. We find that the elastic nonlinearity of angular sand particles is of the same order of magnitude as that previously measured in spherical glass beads. However, while the elastic nonlinearity of glass beads increases by an order of magnitude with RH, that of sand particles is rather RH independent. We attribute this difference to the angularity of sand particles: absorbed water on the spherical grains weakens the junctions making them more nonlinear, while no such effect occurs in sand due to grain interlocking. Additionally, for one of the nonlinear parameters that likely arises from shearing/partial slip of the grain junctions, we observe a sharp amplitude threshold in sand which is not observed in glass beads.

Plain Language Summary

Our main goal is to understand the origin of nonlinear elastic effects in granular materials like rocks. These nonlinear effects are critical in part because they are responsible for the small changes in seismic wave speed, and therefore stiffness, of the Earth's crust. Monitoring these changes is important as they might represent predictors of upcoming earthquakes, and they also play a role in the dynamic triggering of earthquakes. Here we study the effect of grain shape and relative humidity (RH) on the nonlinear elastic properties of granular media. To do this, we use granular media of well-controlled grain size and composition, namely angular fine sand particles. We find that their elastic nonlinearity is of the same order of magnitude as that previously measured in spherical glass beads, however, and unlike in glass beads, we observe little to no dependence with RH. We attribute this lack of changes with RH in sand to grain interlocking, and the fact that absorbed water on the grains is unable to weaken the grain junctions and the granular assembly.

1 Introduction

Nonlinear elastic effects arise in solids due to the presence of imperfections at the micro/mesoscopic scale, such as cracks or dislocations (Ostrovsky & Johnson, 2001). Understanding the origins of these nonlinear elastic effects is critical to numerous fields, from geophysics (Abeele et al., 2002; Delorey et al., 2021; Feng et al., 2018, 2022; Guyer & Johnson, 2009; Hillers et al., 2015; P. Johnson & Sutin, 2005; Manogharan et al., 2021; McCall & Guyer, 1994; Shokouhi et al., 2020; Tadavani et al., 2020; TenCate et al., 1996, 1996, 2016) and civil engineering (Abeele & De Visscher, 2000; Astorga et al., 2018; Bittner & Popovics, 2022; G. Kim et al., 2017; Lacouture et al., 2003; Payan et al., 2014; Shokouhi et al., 2017) to the non-destructive evaluation of materials (Breazeale & Ford, 1965; Buck et al., 1978; Jin et al., 2020; J.-Y. Kim et al., 2006; Matlack et al., 2015; Williams et al., 2022). Elastic nonlinearity is particularly large in poorly consolidated or unconsolidated materials, where it arises from weak junctions between grains (Brunet et al., 2008; Guyer & Johnson, 1999, 2009; Jia et al., 2011; P. A. Johnson & Jia, 2005; Langlois & Jia, 2014; Renaud et al., 2012; Rivière et al., 2015).

Earlier studies have found that the nonlinear elastic response of rocks likely arises from two distinct mechanisms, one that might be related to the opening/closing of grain contacts, and the other one related to the shearing of grain junctions (Renaud et al., 2012; Rivière et al., 2015). To confirm this hypothesis and better understand the underlying physics, we seek to investigate the nonlinear elastic response of materials simpler than rocks, both in terms of composition and microstructural features. In our previous work (Gao et al., 2022), we studied the influence of relative humidity (RH) on the nonlinear elastic properties of glass bead samples, and found that all nonlinear parameters increase by roughly an order of magnitude when RH increases from ~10 % to ~100 %. This implies that, if indeed both mechanisms exist, they are affected in a similar way in glass beads and cannot be disentangled using RH changes. In this study, we further attempt to distinguish both mechanisms, by investigating the role of grain shape on the nonlinear elastic properties of granular media. We use a pump-probe experimental approach called Dynamic Acousto-Elastic Testing (DAET) to extract the full nonlinear elastic response (Renaud et al., 2009, 2011) of granular assemblies made of fine angular sand particles; and unlike our previous study in glass beads, we also vary the RH level. We hypothesize that shearing of grain junctions in samples composed of angular grains is more hindered than in samples made of spherical grains.

2 Materials and Methods

We utilize granular assemblies made of angular, fine quartz sand (diameter 50-150μm, 99.8% SiO_2 with minor amounts of Fe_2O_3, Al_2O_3, <0.1% each, U.S. Silica Company) using a setup identical to our previous study (Fig. 1a) (Gao et al., 2022). We place a 4.5 mm thick pack of particles on top of a steel forcing block of area 10*10 cm^2. A layer of tape is used on the four sides of the block to prevent the particles from escaping. The sample is left overnight in a sealed bag with either desiccants or a 100% RH humid environment, for dry (~10% RH) and humid (100% RH) samples, respectively. We then quickly take the sample out of the sealed bag and place a second steel block of identical size on top of the granular layer. The four sides are then sealed using additional layers of tape. Next, we place two P-wave ultrasonic sensors (central

frequency of 1 MHz, 2.54 cm in diameter, V102-RM from Olympus, Waltham, MA) at the bottom of blind holes inside the steel blocks, each 1.8 mm away from the granular sample. A thin layer of molasses is added to ensure proper ultrasonic coupling between the ultrasonic transducers and the steel blocks. The sample assembly is then placed inside a loading apparatus. An on-board direct current displacement transducer (DCDT) is attached to the top steel block and used to measure changes in thickness throughout the experiment. A load cell is placed in series between the sample and the hydraulic ram to measure force/stress. We conduct 14 experiments in sand at various levels of relative humidity (dry ~10 %, ambient 30 %~70 %, and humid ~100 %).

A static stress of 4 MPa is first applied to the sample with a hydraulic ram and is maintained constant throughout the experiment via servocontrol. Dynamic oscillations are then superimposed to the static stress, also via servocontrol. We first apply two oscillation sets with 0.3 MPa peak amplitude for initial compaction and homogenization. Then we conduct four identical DAET oscillation sets, each made of 15 oscillations with peak amplitudes linearly increasing from 0.01 MPa to 0.3 MPa. Each oscillation is made of 50 sinusoidal cycles at a fixed frequency of 10 Hz, separated by 20-second hold intervals. Detailed plots of stress and thickness versus time are shown in Fig. S1.

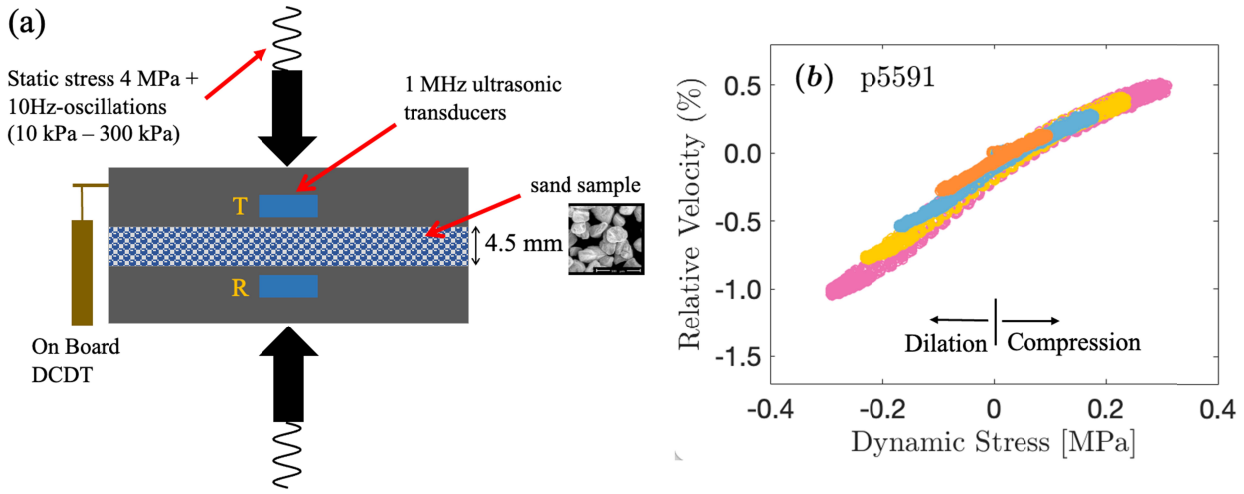

Figure 1. Experimental setup and typical result. (a) Experimental setup showing the loading apparatus and sample assembly. Full scale scanning electron microscopy (SEM) images are shown in Fig. S2. (b) Typical nonlinear signatures (experiment p5591 is for a sample at 100% RH). Only 4 out of 15 dynamic stress levels are shown for clarity. The signatures for all sand samples are shown in Fig. S3.

3 Data Analysis

After applying static stress to the sample, we measure the initial layer thickness with a caliper. We hand-pick the first arrival of a reference waveform (average of 50 consecutive waveforms taken after applying static stress) to estimate the initial time-of-flight. We then use thickness

changes Δh measured with the displacement sensor and time-of-flight changes Δt estimated using cross-correlation to calculate the wave velocity c throughout the experiment (Gao et al., 2022). Next, we compute the relative wave velocity change $\Delta c/c = (c_{osc} - c_0)/c_0$ for each individual oscillation, where c_0 and c_{osc} are the pre-oscillation wave velocity and the wave velocity during the oscillation, respectively (Fig. S4). We can then generate the so-called nonlinear signatures by plotting relative velocity change $\Delta c/c$ as a function of dynamic stress (Fig. 1b).

Next, to determine the type and amount of nonlinearity, the $\Delta c/c$ vs time signals are projected onto a basis of sine and cosine functions at frequencies nf $(n = 0, 1, 2)$, where f is the oscillation frequency (10 Hz). We then use these Fourier coefficients to calculate the magnitude of the harmonics R_n. Using n up to 2 for these sand samples is sufficient to capture the complexity of the nonlinear signatures, similar to what had been observed in glass beads (Gao et al., 2022). The parameter R_0 characterizes the average softening taking place during the oscillations (Fig. S4c), while the parameters R_1 and R_2 are related to the amount of slope and curvature in the nonlinear signatures, respectively (Fig.1b and Fig. S3). After extracting the harmonic amplitudes for each nonlinear signature, we look at their evolution with respect to the peak stress amplitude σ using a general power-law of the form:

$$R_n = a_n \sigma^{\nu_n} \quad (1)$$

where the power exponent ν represents the type of nonlinearity (and associated physical mechanism), while the coefficient a represents how much of this mechanism or nonlinearity type is present. Finally, because we plot R_n as a function of σ in a log-log fashion, the exponent ν will be assessed by evaluating the slope, while the parameter a will be extracted using the y-intercept $\log(a_n)$, following:

$$\log(R_n) = \nu_n \log(\sigma) + \log(a_n). \quad (2)$$

4 Results and Discussion

Typical nonlinear signatures at four dynamic stress amplitudes are shown in Fig. 1b. Similar plots for all 14 sand samples are shown in Figs. S3. They all exhibit a similar positive correlation between wave velocity and dynamic stress, where, as expected, the wave velocity is larger when dynamic stress is positive (compression phase), and smaller when dynamic stress is negative (dilation phase). We also observe that the slope (R_1 component) of the signature dominate the shape of the signature compared to the offset (R_0 component) and curvature (R_2 component), which is typical when the pump and probe are aligned (vertical direction here, see Fig. 1a) (Renaud et al., 2013). Some rather large hysteresis can be observed for some of the samples, irrespective of RH level or grain shape. The reason behind the variability in hysteresis size is not clear and additional work would be required. Finally, we observe that for some samples, the slope appears larger during the dilation phase than during compression, suggesting that during the compression phase, the grain junctions are more tightly closed, producing smaller velocity changes.

To obtain a quantitative assessment of the effect of grain shape and RH, we extract the harmonic content of all signatures. We calculate the Fourier series coefficients from the $\Delta c/c$ vs time signals at frequencies nf where f is the pump frequency (10 Hz) and $n = 0, 1, 2$. These coefficients, called R_n and representing the harmonic content, are shown in Fig. 2d-2f as a function of peak dynamic stress amplitude for all sand samples. Moreover, to help us examine the effect of grain shape, we plot previous data obtained in glass beads under the same experimental conditions for comparison (Fig. 2a-2c) (Gao et al., 2022). On these log-log plots, following Eq. 2, the slope tells us about the nonlinearity type (ν_n) while the y-intercept ($\log(a_n)$) indicates the amount of nonlinearity for that particular type. We see that in glass beads, the R_n values are larger in fully humid samples than in drier samples, while in sand, all the curves seem to overlap, that is, the nonlinearity level seems rather independent of RH. For both sample types, the R_0 and R_1 values fit roughly linearly ($\nu_0 \approx 1$, $\nu_1 \approx 1$) with dynamic stress amplitude. Such scalings for R_0 and R_1 suggest that the y-intercepts on these plots correspond to the hysteretic and quadratic nonlinear parameters α and β, respectively. As for the R_2 values, they scale roughly quadratically ($\nu_2 \approx 2$), which suggests that the y-intercept corresponds to the cubic nonlinear parameter δ. Note that for sand, R_2 is rather stress-independent at low stress and starts to increase quadratically only above ~0.1-0.2 MPa (as indicated by the small vertical arrow in Fig. 2f). Based on these scalings, we overlay parallel lines to indicate the value of each nonlinear parameter for a given y-intercept. The three nonlinear parameters α, β and δ dictate the strain-dependence of the elastic modulus M (or equivalently the wave velocity c) according to:

$$\frac{\Delta M}{M_0} = 2\frac{\Delta c}{c_0} = \beta\varepsilon + \delta\varepsilon^2 + \alpha(\varepsilon_0 + \mathrm{sign}(\dot{\varepsilon})\varepsilon)$$

where ε is the dynamic strain, $\dot{\varepsilon}$ is the strain rate, and ε_0 is the dynamic strain amplitude. Because our controlling variable is stress rather than strain, we convert from strain to stress assuming that the nonlinearity is small, i.e., $\sigma = M_0\varepsilon$, where $M_0 = 1$ GPa which corresponds to an average linear elastic modulus for all samples. This allows us to compare the nonlinear parameters with values found in the existing literature where, most of the time, the controlling variable is strain (Guyer & Johnson, 2009).

Harmonic amplitude plots of all sand samples, sorted per samples rather than R_n values, are also included in the supplementary materials (Fig. S6). For both sample types, at a given dynamic stress amplitude, we find that R_1 is larger than R_0 and R_2, which is consistent with our previous observation that the slope dominates the nonlinear signatures compared to the offset and the curvature.

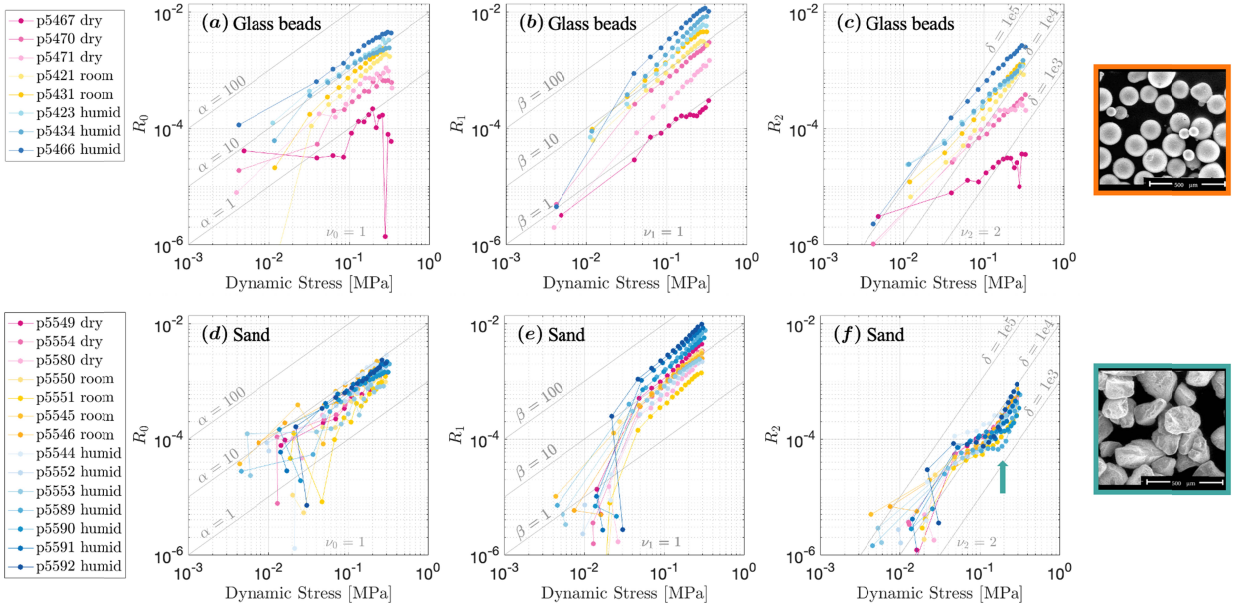

Figure 2. Harmonic amplitudes R_n as a function of dynamic stress amplitude. The top row shows results previously obtained in glass beads (Gao et al., 2022), while the bottom row shows data collected in sand. We only also show results from the third DAET test for clarity. (a-d) Parameter R_0. The overall scaling is linear [$\nu_0 \approx 1$ in Eq. (2)]. (b-e) Parameter R_1. The overall scaling is roughly linear [$\nu_1 \approx 1$ in Eq. (2)]. (c-f) Parameter R_2. The scaling is approximately quadratic [$\nu_2 \approx 2$ in Eq. (2)]. Note the kink in the curves at ~0.2 MPa for the sand samples – panel f – as pointed out by the small vertical arrow (also see Fig. 4).

We plot the extracted nonlinear parameters α, β, and δ as a function of RH level in Fig. 3. Again, results for both sand and glass beads are reported for comparison. We find that overall, both materials have a similar range of elastic nonlinearity. However, while all nonlinear parameters increase with RH for glass beads, little variation can be seen in sand. For sand, α and δ exhibit no variation with RH, and only a small increase in β for fully humid samples, on

average, although scatter is quite large. We do not know if this increase in β at 100% RH is real or due to the large scatter; we conducted more experiments at 100% RH than at drier conditions, so the scatter might appear larger for that reason. We are currently designing a new setup where a single sample kept under static load can be monitored while being humidified/dried. By doing so, we anticipate reducing uncertainties by monitoring the elastic nonlinearity of a single sample instead of different samples.

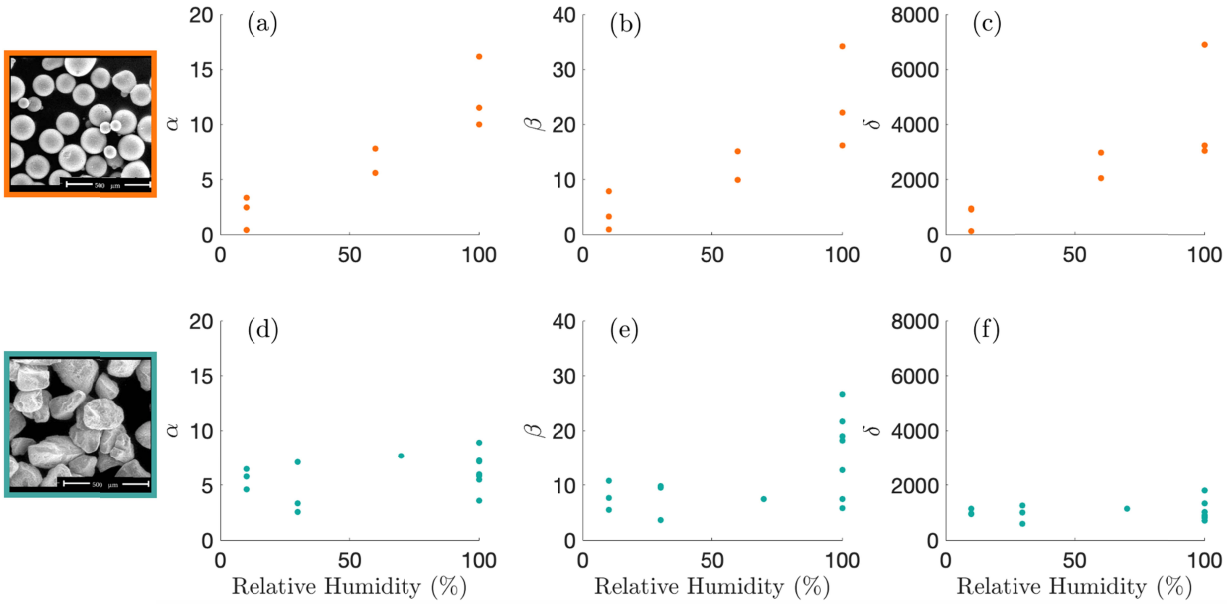

Figure 3. Nonlinear parameters as a function of RH. The top row shows results previously obtained in glass beads (Gao et al., 2022), while the bottom row shows results obtained in sand. These parameters are related to a_n in Eq. (2), that is, (a)(d) α related to a_0, (b)(e) β related to a_1, and (c)(f) δ related to a_2. Each point represents one DAET test (four tests per experiment). Notice how all nonlinear parameters increase with RH for glass beads, while they are rather independent of RH in sand.

As discussed in the introduction, previous studies (Renaud et al., 2012; Rivière et al., 2015, 2016) suggest that there exists two main physical mechanisms behind the nonlinear elastic properties of granular/damaged solids: the parameter β, (related to R_1) which that is likely related to the opening/closing of cracks and grain-grain junctions; while all other parameters (α, related to R_0; δ, related to R_2 as well as hysteresis area (Renaud et al., 2012; Rivière et al., 2015) might be related to shearing/partial slip of these same features. In this work, we find that the nonlinear parameters are rather independent of RH in sand, in contrast with the strong dependence observed in glass beads (Gao et al., 2022). This is in line with the interpretation made in our previous study (Gao et al., 2022), hypothesizing that adsorbed water on glass beads pushes the beads apart (similar to a small increase in pore pressure (Gor & Gurevich, 2018; Gor & Neimark, 2010), making the junctions weaker and more nonlinear. The fact that the elastic nonlinearity does not significantly change with RH in sand might come from grain interlocking, that is, the angular grains prevent adsorbed water from weakening/dilating the sample. Previous

results in porous sandstones have shown that adsorbed water on the grains causes tensile deformation and reduced elastic moduli (Amberg & McIntosh, 1952; Guyer & Kim, 2015; Yurikov et al., 2018), although the grains are angular. This is in contradiction with our results in unconsolidated sand, where changes in RH have little effect, but seems to suggest that in sandstones, the changes in RH affect the soft bonds between the grains, rather the bare contacts between grains.

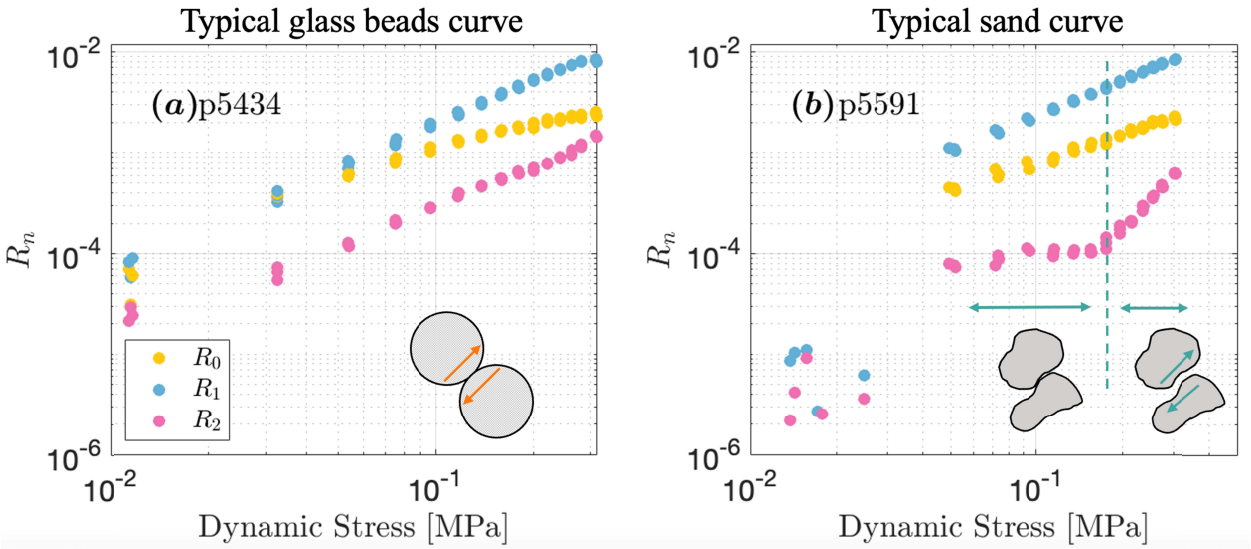

Figure 4. Harmonic amplitudes extracted from the nonlinear signatures on a log-log scale. The parameter R_0 represents the transient elastic weakening, while R_1 and R_2 is related to the slope and curvature of the nonlinear signatures. (a) A typical glass bead sample at 100% RH (Gao et al., 2022)(b) A typical sand sample at 100% RH.

Finally, we emphasize our previous observation that in sand samples, the parameter R_2 is stress-independent at low dynamic stress amplitudes and starts to increase quadratically for amplitudes larger than ~0.1–0.2 MPa (small arrow in Fig. 3f). In Fig. 4, we show the R_n values vs dynamic stress amplitude for one typical glass bead sample (Fig. 4a) and one typical sand sample (Fig. 4b). We see a clear kink in the curve for R_2 in sand, while it increases monotonically with stress amplitude in glass beads. If R_2, related to the curvature of the nonlinear signatures and the parameter δ, originates from shearing/partial slip of the grain junctions – as we argue – then this suggests that shearing/partial slip is mostly absent at low stress/strain amplitudes due to grain locking, and starts taking place only above a particular stress amplitude (~0.1–0.2 MPa here). In comparison, shearing/partial slip in spherical glass beads likely initiates at much lower dynamic stress/strain amplitudes. Another interesting observation is that other R_n values in sand do not exhibit any such amplitude threshold. Because previous work suggests that β/R_1 is related to one mechanism while all other parameters are related to a second mechanism, we could have expected both R_0 and R_2 to exhibit an amplitude threshold. This is not the case and further work would be needed to investigate this discrepancy.

5 Conclusions

In this study, we investigate the effect of grain shape and relative humidity on the nonlinear elastic properties of granular media by conducting experiments on angular quartz sand, and by comparing them with results previously obtained in spherical glass beads (Gao et al., 2022). We found that, compared to glass beads, the elastic nonlinearity of angular sand does not increase significantly with RH, but is rather independent of RH, which we attribute to grain interlocking that prevents adsorbed water from weakening the grain junctions. Furthermore, for one of the nonlinear parameters (δ/R_2) which has been attributed to sliding/partial slip of grain junctions, we observe a sharp amplitude threshold in sand not observed in glass beads. This seems to confirm that this nonlinear parameter (δ/R_2) is indeed related to sliding/partial slip of the grain junctions. Below the amplitude threshold, i.e., at low dynamic stress oscillations, the angular grains of sand are locked, and no sliding/partial slip can occur. This mechanism seems to get activated only at larger stress oscillations when the grain junctions unlock.

Acknowledgments

The authors would like to thank Chris Marone for his help with the loading apparatus and many helpful discussions, Steve Swavely for technical support, and David C. Bolton, Srisharan Shreedharan, Clay Wood, Samson Marty, and Raphael Affinito for their help with operating the loading apparatus. This work was partially supported by a grant from the U.S. Department of Energy, Office of Basic Energy Sciences (Award Number DE-SC0017585) to PS, and a grant from the U.S. Department of Energy, Office of Basic Energy Sciences (Award Number DE-SC0022842) to JR.

Open Research

The data and code used in the study are available at Penn State University's Scholar Sphere via [doi:10.26207/ppqc-7d70, https://scholarsphere.psu.edu/resources/0d041b4d-57c9-457c-9525-a7282c63e5f8] with all rights reserved.

References

Abeele, K. V. D., & De Visscher, J. (2000). Damage assessment in reinforced concrete using spectral and temporal nonlinear vibration techniques. *Cement and Concrete Research*, *30*(9), 1453–1464. https://doi.org/10.1016/S0008-8846(00)00329-X

Abeele, K. V. D., Carmeliet, J., Johnson, P. A., & Zinszner, B. (2002). Influence of water saturation on the nonlinear elastic mesoscopic response in Earth materials and the implications to the mechanism of nonlinearity. *Journal of Geophysical Research: Solid Earth*, *107*(B6), ECV 4-1-ECV 4-11. https://doi.org/10.1029/2001JB000368

Amberg, C. H., & McIntosh, R. (1952). A study of adsorption hysteresis by means of length changes of a rod of porous glass. *Canadian Journal of Chemistry*, *30*(12), 1012–1032. https://doi.org/10.1139/v52-121

Astorga, A., Guéguen, P., & Kashima, T. (2018). Nonlinear Elasticity Observed in Buildings during a Long Sequence of Earthquakes. *Bulletin of the Seismological Society of America*, *108*(3A), 1185–1198. https://doi.org/10.1785/0120170289

Bittner, J. A., & Popovics, J. S. (2022). Transient nonlinear vibration characterization of building materials in sequential impact scale experiments. *Frontiers in Built Environment*, *8*, 949484. https://doi.org/10.3389/fbuil.2022.949484

Breazeale, M. A., & Ford, J. (1965). Ultrasonic Studies of the Nonlinear Behavior of Solids. *Journal of Applied Physics*, *36*(11), 3486–3490. https://doi.org/10.1063/1.1703023

Brunet, T., Jia, X., & Johnson, P. A. (2008). Transitional nonlinear elastic behaviour in dense granular media. *Geophysical Research Letters*, *35*(19). https://doi.org/10.1029/2008GL035264

Buck, O., Morris, W. L., & Richardson, J. M. (1978). Acoustic harmonic generation at unbonded interfaces and fatigue cracks. *Applied Physics Letters*, *33*(5), 371–373. https://doi.org/10.1063/1.90399

Delorey, A. A., Guyer, R. A., Bokelmann, G. H. R., & Johnson, P. A. (2021). Probing the Damage Zone at Parkfield. *Geophysical Research Letters*, *48*(13), e2021GL093518. https://doi.org/10.1029/2021GL093518

Feng, X., Fehler, M., Brown, S., Szabo, T. L., & Burns, D. (2018). Short-Period Nonlinear Viscoelastic Memory of Rocks Revealed by Copropagating Longitudinal Acoustic Waves. *Journal of Geophysical Research: Solid Earth*, *123*(5), 3993–4006. https://doi.org/10.1029/2017JB015012

Feng, X., Fehler, M., Burns, D., Brown, S., & Szabo, T. L. (2022). Effects of humidity and temperature on the non-linear elasticity of rocks. *Geophysical Journal International*, *231*(3), 1823–1832. https://doi.org/10.1093/gji/ggac292

Gao, L., Shokouhi, P., & Rivière, J. (2022). Effect of relative humidity on the nonlinear elastic response of granular media. *Journal of Applied Physics*, *131*(5), 055101. https://doi.org/10.1063/5.0073967

Gor, G. Y., & Gurevich, B. (2018). Gassmann Theory Applies to Nanoporous Media. *Geophysical Research Letters*, *45*(1), 146–155. https://doi.org/10.1002/2017GL075321

Gor, G. Y., & Neimark, A. V. (2010). Adsorption-Induced Deformation of Mesoporous Solids. *Langmuir*, *26*(16), 13021–13027. https://doi.org/10.1021/la1019247

Guyer, R. A., & Johnson, P. A. (1999). Nonlinear Mesoscopic Elasticity: Evidence for a New Class of Materials. *Physics Today*, *52*(4), 30–36. https://doi.org/10.1063/1.882648

Guyer, R. A., & Johnson, P. A. (2009). *Nonlinear Mesoscopic Elasticity*. Weinheim, Germany: Wiley-VCH Verlag GmbH & Co. KGaA. https://doi.org/10.1002/9783527628261

Guyer, R. A., & Kim, H. A. (2015). Theoretical model for fluid-solid coupling in porous materials. *Physical Review E*, *91*(4), 042406. https://doi.org/10.1103/PhysRevE.91.042406

Hillers, G., Retailleau, L., Campillo, M., Inbal, A., Ampuero, J.-P., & Nishimura, T. (2015). In situ observations of velocity changes in response to tidal deformation from analysis of the high-frequency ambient wavefield. *Journal of Geophysical Research: Solid Earth*, *120*(1), 210–225. https://doi.org/10.1002/2014JB011318

Jia, X., Brunet, Th., & Laurent, J. (2011). Elastic weakening of a dense granular pack by acoustic fluidization: Slipping, compaction, and aging. *Physical Review E*, *84*(2), 020301. https://doi.org/10.1103/PhysRevE.84.020301

Jin, J., Johnson, P. A., & Shokouhi, P. (2020). An integrated analytical and experimental study of contact acoustic nonlinearity at rough interfaces of fatigue cracks. *Journal of the Mechanics and Physics of Solids*, *135*, 103769. https://doi.org/10.1016/j.jmps.2019.103769

Johnson, P., & Sutin, A. (2005). Slow dynamics and anomalous nonlinear fast dynamics in diverse solids. *The Journal of the Acoustical Society of America*, *117*(1), 124–130. https://doi.org/10.1121/1.1823351

Johnson, P. A., & Jia, X. (2005). Nonlinear dynamics, granular media and dynamic earthquake triggering. *Nature*, *437*(7060), 871–874. https://doi.org/10.1038/nature04015

Kim, G., Kim, J.-Y., Kurtis, K. E., & Jacobs, L. J. (2017). Drying shrinkage in concrete assessed by nonlinear ultrasound. *Cement and Concrete Research*, *92*, 16–20. https://doi.org/10.1016/j.cemconres.2016.11.010

Kim, J.-Y., Jacobs, L. J., Qu, J., & Littles, J. W. (2006). Experimental characterization of fatigue damage in a nickel-base superalloy using nonlinear ultrasonic waves. *The Journal of the Acoustical Society of America*, *120*(3), 1266–1273. https://doi.org/10.1121/1.2221557

Lacouture, J.-C., Johnson, P. A., & Cohen-Tenoudji, F. (2003). Study of critical behavior in concrete during curing by application of dynamic linear and nonlinear means. *The Journal of the Acoustical Society of America*, *113*(3), 1325–1332. https://doi.org/10.1121/1.1543927

Langlois, V., & Jia, X. (2014). Acoustic probing of elastic behavior and damage in weakly cemented granular media. *Physical Review E*, *89*(2), 023206. https://doi.org/10.1103/PhysRevE.89.023206

Manogharan, P., Wood, C., Marone, C., Elsworth, D., Rivière, J., & Shokouhi, P. (2021). Nonlinear elastodynamic behavior of intact and fractured rock under in-situ stress and saturation conditions. *Journal of the Mechanics and Physics of Solids*, *153*, 104491. https://doi.org/10.1016/j.jmps.2021.104491

Matlack, K. H., Kim, J.-Y., Jacobs, L. J., & Qu, J. (2015). Review of Second Harmonic Generation Measurement Techniques for Material State Determination in Metals. *Journal of Nondestructive Evaluation*, *34*(1), 273. https://doi.org/10.1007/s10921-014-0273-5

McCall, K. R., & Guyer, R. A. (1994). Equation of state and wave propagation in hysteretic nonlinear elastic materials. *Journal of Geophysical Research: Solid Earth*, *99*(B12), 23887–23897. https://doi.org/10.1029/94JB01941

Ostrovsky, L. A., & Johnson, P. A. (2001). Dynamic nonlinear elasticity in geomaterials. *La Rivista Del Nuovo Cimento*, *24*(7), 1–46. https://doi.org/10.1007/BF03548898

Payan, C., Ulrich, T. J., Le Bas, P. Y., Saleh, T., & Guimaraes, M. (2014). Quantitative linear and nonlinear resonance inspection techniques and analysis for material characterization: Application to concrete thermal damage. *The Journal of the Acoustical Society of America*, *136*(2), 537–546. https://doi.org/10.1121/1.4887451

Renaud, G., Callé, S., & Defontaine, M. (2009). Remote dynamic acoustoelastic testing: Elastic and dissipative acoustic nonlinearities measured under hydrostatic tension and compression. *Applied Physics Letters*, *94*(1), 011905. https://doi.org/10.1063/1.3064137

Renaud, G., Le Bas, P., Ten Cate, J. A., Ulrich, T. J., Carey, J. W., Han, J., et al. (2011). Dynamic Measures of Elastic Nonlinear (Anelastic) Behavior: Dynamic Acousto-Elasticity Testing (DAET). *AGU Fall Meeting Abstracts*, *51*, MR51A-2151.

Renaud, G., Le Bas, P.-Y., & Johnson, P. A. (2012). Revealing Highly Complex Elastic Nonlinear (anelastic) Behavior of Earth Materials Applying a New Probe: Dynamic Acoustoelastic Testing: A New Probe for Elasticity in Rocks. *Journal of Geophysical Research: Solid Earth*, *117*(B6). https://doi.org/10.1029/2011JB009127

Renaud, G., Rivière, J., Haupert, S., & Laugier, P. (2013). Anisotropy of dynamic acoustoelasticity in limestone, influence of conditioning, and comparison with nonlinear resonance spectroscopy. *The Journal of the Acoustical Society of America*, *133*(6), 3706–3718. https://doi.org/10.1121/1.4802909

Rivière, J., Shokouhi, P., Guyer, R. A., & Johnson, P. A. (2015). A set of measures for the systematic classification of the nonlinear elastic behavior of disparate rocks. *Journal of*

Geophysical Research: Solid Earth, *120*(3), 1587–1604. https://doi.org/10.1002/2014JB011718

Rivière, J., Pimienta, L., Scuderi, M., Candela, T., Shokouhi, P., Fortin, J., et al. (2016). Frequency, pressure, and strain dependence of nonlinear elasticity in Berea Sandstone. *Geophysical Research Letters*, *43*(7), 3226–3236. https://doi.org/10.1002/2016GL068061

Shokouhi, P., Rivière, J., Lake, C. R., Le Bas, P.-Y., & Ulrich, T. J. (2017). Dynamic acousto-elastic testing of concrete with a coda-wave probe: comparison with standard linear and nonlinear ultrasonic techniques. *Ultrasonics*, *81*, 59–65. https://doi.org/10.1016/j.ultras.2017.05.010

Shokouhi, P., Jin, J., Wood, C., Rivière, J., Madara, B., Elsworth, D., & Marone, C. (2020). Dynamic Stressing of Naturally Fractured Rocks: On the Relation Between Transient Changes in Permeability and Elastic Wave Velocity. *Geophysical Research Letters*, *47*(1), e2019GL083557. https://doi.org/10.1029/2019GL083557

Tadavani, S. K., Poduska, K. M., & Malcolm, A. E. (2020). A non-linear elastic approach to study the effect of ambient humidity on sandstone. *Journal of Applied Physics*, *128*(24), 244902. https://doi.org/10.1063/5.0025936

TenCate, J. A., Abeele, K. V. D., Shankland, T. J., & Johnson, P. A. (1996). Laboratory study of linear and nonlinear elastic pulse propagation in sandstone. *The Journal of the Acoustical Society of America*, *100*(3), 1383–1391. https://doi.org/10.1121/1.415985

TenCate, J. A., Malcolm, A. E., Feng, X., & Fehler, M. C. (2016). The effect of crack orientation on the nonlinear interaction of a *P* wave with an *S* wave. *Geophysical Research Letters*, *43*(12), 6146–6152. https://doi.org/10.1002/2016GL069219

Williams, C., Borigo, C., Rivière, J., Lissenden, C. J., & Shokouhi, P. (2022). Nondestructive Evaluation of Fracture Toughness in 4130 Steel Using Nonlinear Ultrasonic Testing. *Journal of Nondestructive Evaluation*, *41*(1), 13. https://doi.org/10.1007/s10921-022-00846-5

Yurikov, A., Lebedev, M., Gor, G. Y., & Gurevich, B. (2018). Sorption-Induced Deformation and Elastic Weakening of Bentheim Sandstone. *Journal of Geophysical Research: Solid Earth*, *123*(10), 8589–8601. https://doi.org/10.1029/2018JB016003